Research Article | Vol. 26, No. 18 | 3 Sep 2018 | OPTICS EXPRESS 23426
Optics EXPRESS

Mesoscale surface plasmons: modelling and imaging using near-field scanning optical microscopy

ARI D. MAYEVSKY,[1] TIMOTHY J. DAVIS,[2] PATRYCJA M. BALLARD,[1] CLARE A. HENDERSON,[1] AND ALISON M. FUNSTON[1,*]

[1]*ARC Centre of Excellence in Exciton Science and School of Chemistry, Monash University, Clayton, Victoria 3800, Australia*
[2]*School of Physics, University of Melbourne, Parkville, Victoria 3010, Australia*
[*]*alison.funston@monash.edu*

Abstract: Meso-scale plasmons are supported by structures with dimensions on the order of tens of plasmon wavelengths. Metal structures at this length-scale are promising for the design and engineering of structures to direct the flow of optical energy and generate high intensity, localized electric fields. The near-field optical properties of meso-scale crystalline gold plates were examined using near-field scanning optical microscopy with a focus on the effects of modifying morphology and excitation conditions. Excitation of surface plasmon polaritons (SPPs) at plate edges and their subsequent propagation and interference as radial waves across the surface results in nodes of enhancement of the near-field on the plate surface at specific positions within the plate. The spatial position of the near-field enhancement may be directed by controlling either, or both, the boundary conditions (plate shape) and polarization of the excitation light.

OCIS codes: (240.6680) Surface plasmons; (240.5420) Polaritons; (180.4243) Near-field microscopy.

References and links

1. S. A. Maier, *Plasmonics: Fundamentals and Applications* (Springer US, New York, NY, 2007).
2. S. A. Maier, P. G. Kik, and H. A. Atwater, "Observation of coupled plasmon-polariton modes in Au nanoparticle chain waveguides of different lengths: Estimation of waveguide loss," Appl. Phys. Lett. **81**, 1714–1716 (2002).
3. V. K. Valev, A. V. Silhanek, B. De Clercq, W. Gillijns, Y. Jeyaram, X. Zheng, V. Volskiy, O. A. Aktsipetrov, G. A. E. Vandenbosch, M. Ameloot, V. V. Moshchalkov, and T. Verbiest, "U-Shaped Switches for Optical Information Processing at the Nanoscale," Small **7**, 2573–2576 (2011).
4. T. J. Davis and D. E. Gómez, "Colloquium : An algebraic model of localized surface plasmons and their interactions," Rev. Mod. Phys. **89**, 011003 (2017).
5. M. Kuttge, E. J. R. Vesseur, J. Verhoeven, H. J. Lezec, H. A. Atwater, and A. Polman, "Loss mechanisms of surface plasmon polaritons on gold probed by cathodoluminescence imaging spectroscopy." Appl. Phys. Lett. **93**, 113110 (2008).
6. T. A. Major, M. S. Devadas, S. S. Lo, and G. V. Hartland, "Optical and Dynamical Properties of Chemically Synthesized Gold Nanoplates," J. Phys. Chem. C **117**, 1447–1452 (2013).
7. G. Beane, K. Yu, T. Devkota, P. Johns, B. Brown, G. P. Wang, and G. Hartland, "Surface Plasmon Polariton Interference in Gold Nanoplates," J. Phys. Chem. Lett. **8**, 4935–4941 (2017).
8. D. Rossouw, M. Couillard, J. Vickery, E. Kumacheva, and G. A. Botton, "Multipolar Plasmonic Resonances in Silver Nanowire Antennas Imaged with a Subnanometer Electron Probe," Nano Lett. **11**, 1499–1504 (2011).
9. D. Rossouw and G. A. Botton, "Resonant optical excitations in complementary plasmonic nanostructures," Opt. Express **20**, 6968 (2012).
10. F.-P. Schmidt, H. Ditlbacher, U. Hohenester, A. Hohenau, F. Hofer, and J. R. Krenn, "Universal dispersion of surface plasmons in flat nanostructures," Nat. Commun. **5**, 3604 (2014).
11. B. Frank, P. Kahl, D. Podbiel, G. Spektor, M. Orenstein, L. Fu, T. Weiss, M. Horn-von Hoegen, T. J. Davis, F.-J. Meyer zu Heringdorf, and H. Giessen, "Short-range surface plasmonics: Localized electron emission dynamics from a 60-nm spot on an atomically flat single-crystalline gold surface," Sci. Adv. **3**, e1700721 (2017).
12. J. Nelayah, M. Kociak, O. Stéphan, F. J. García de Abajo, M. Tencé, L. Henrard, D. Taverna, I. Pastoriza-Santos, L. M. Liz-Marzán, and C. Colliex, "Mapping surface plasmons on a single metallic nanoparticle," Nat. Phys. **3**, 348–353 (2007).
13. F.-P. Schmidt, H. Ditlbacher, U. Hohenester, A. Hohenau, F. Hofer, and J. R. Krenn, "Dark Plasmonic Breathing Modes in Silver Nanodisks," Nano Lett. **12**, 5780–5783 (2012).
14. H. Duan, A. I. Fernández-Domínguez, M. Bosman, S. A. Maier, and J. K. W. Yang, "Nanoplasmonics: Classical down to the Nanometer Scale," Nano Lett. **12**, 1683–1689 (2012).

#328987 https://doi.org/10.1364/OE.26.023426
Received 3 May 2018; revised 6 Aug 2018; accepted 9 Aug 2018; published 28 Aug 2018

Optics EXPRESS

15. C. Eggeling, J. Schaffer, C. a. M. Seidel, J. Korte, G. Brehm, S. Schneider, and W. Schrof, "Homogeneity, Transport, and Signal Properties of Single Ag Particles Studied by Single-Molecule Surface-Enhanced Resonance Raman Scattering," J. Phys. Chem. A **105**, 3673–3679 (2001).
16. G. Spektor, D. Kilbane, A. K. Mahro, B. Frank, S. Ristok, L. Gal, P. Kahl, D. Podbiel, S. Mathias, H. Giessen, F.-J. Meyer zu Heringdorf, M. Orenstein, and M. Aeschlimann, "Revealing the subfemtosecond dynamics of orbital angular momentum in nanoplasmonic vortices," Science (80-.). **355**, 1187–1191 (2017).
17. J. A. Veerman, A. M. Otter, L. Kuipers, and N. F. van Hulst, "High definition aperture probes for near-field optical microscopy fabricated by focused ion beam milling," Appl. Phys. Lett. **72**, 3115–3117 (1998).
18. J. M. Atkin, S. Berweger, A. C. Jones, and M. B. Raschke, "Nano-optical imaging and spectroscopy of order, phases, and domains in complex solids," Adv. Phys. **61**, 745–842 (2012).
19. T. J. Davis, B. Frank, D. Podbiel, P. Kahl, F.-J. Meyer zu Heringdorf, and H. Giessen, "Subfemtosecond and Nanometer Plasmon Dynamics with Photoelectron Microscopy: Theory and Efficient Simulations," ACS Photonics **4**, 2461–2469 (2017).
20. Z. Guo, Y. Zhang, Y. DuanMu, L. Xu, S. Xie, and N. Gu, "Facile synthesis of micrometer-sized gold nanoplates through an aniline-assisted route in ethylene glycol solution," Colloids Surfaces A Physicochem. Eng. Asp. **278**, 33–38 (2006).
21. T. Davis, "Surface plasmon modes in multi-layer thin-films," Opt. Commun. **282**, 135–140 (2009).
22. B. Wild, L. Cao, Y. Sun, B. P. Khanal, E. R. Zubarev, S. K. Gray, N. F. Scherer, and M. Pelton, "Propagation Lengths and Group Velocities of Plasmons in Chemically Synthesized Gold and Silver Nanowires," ACS Nano **6**, 472–482 (2012).

1. Introduction

A surface plasmon polariton is a collective oscillation of electric charge density at the surface of a metal, coupled to its electric field in the adjacent dielectric that decays rapidly with distance from the surface [1]. The plasmon may be excited by the electric field component of light and, because of the exponential decay of the plasmon electric field with distance above the metal, it leads to confinement of the absorbed energy close to the metal surface [1]. This property provides the capability to manipulate light below the diffraction limit, enabling the creation of optical components with sizes in the nanometer regime [2, 3].

Surface plasmons are usually divided into two classes: surface plasmon polaritons (SPPs) that propagate relatively large distances as waves over extended surfaces of metal films; and localized surface plasmons (LSPs) that exist as resonances on small metal particles [4]. However, there is an intermediate regime, that we call meso-scale plasmonics, where a structure is large enough to support SPPs but small enough that they do not fully decay before reaching the other side. Meso-scale plasmons exist on metal structures with dimensions on the order of tens of plasmon wavelengths. This scale depends on the crystallinity as single crystal gold structures can have plasmon propagation lengths on the order of ≈50-100 μm [5]. Polycrystalline gold structures, such as those obtained via physical evaporation techniques, have much shorter plasmon propagation lengths of the order of ≈20 μm [5]. Light scattering [6], transient absorption microscopy [7], electron energy loss spectroscopy (EELS) [8–10] and two-photon photoemission electron microscopy [11] have shown that light can be transferred across meso-scale gold plates [6, 7] and that SPP interference plays a major role on in this length regime [7, 11]. These effects are in contrast to plate-like structures with dimensions on the order of tens to a few hundreds of nanometers, whose optical properties are controlled primarily through LSP resonance effects [12, 13]. While scaling rules which relate the SPP modes of a film surface and edge to modes in nanodisks supporting LSPs have been suggested, these do not directly address meso-scale structures and only hold for circular nanodisks [10].

One of the major goals in designing sub-wavelength optical components is to engineer structures that generate high intensity, localized electric field spots [14] that can be used in sensing or for applications with SERS [15]. Because of this, focussed ion beams have been used to fabricate meso-scale structures for plasmon focussing [11] or to induce plasmon orbital angular momentum [16]. On a meso-scale metallic plate, plasmons may be excited at all boundaries which then propagate inwards to create complex interference patterns. A more complete understanding

Optics EXPRESS

of the means by which the optical properties in meso-scale plasmonics can be modified provides a basis for structure design.

Near-field Scanning Optical Microscopy (NSOM) is a probe-based technique where a metal-coated fibre optic with a nanoscale aperture (down to ≈20 nm) at the tip [17] is scanned over a surface. The aperture allows coupling of the local field into the fibre, which transports the signal to a detector [18]. As this coupling depends on the aperture on the tip, the optical signal has a spatial resolution defined by the aperture size [17]. The optical detection and the atomic force microscope (AFM) scans occur simultaneously via the probe, allowing the sample morphology to be co-localized with the near-field optical responses.

In this work, we study the interference patterns of SPPs on meso-scale crystalline gold plates using NSOM. The SPPs are initiated at the boundaries using continuous wave light sources with different polarization conditions, and this controls the in-coupling of plasmon waves at different plate boundaries. A model of the SPP electric field and its initiation at the boundaries by the incident light wave was recently developed for analysing 2PPE-PEEM (two-photon photo-emission photo-emission electron microscopy) experiments [19]. This model is modified to describe SPP waves initiated by a single continuous wave, such as that of a CW laser, and results are compared with experiment. Importantly, we show that the boundary and polarization conditions can control the energy flow over the surface leading to control of the location of regions of SPP enhancement.

2. Experimental section

2.1. Materials

Ethylene Glycol (EG, > 99.8%), aniline (> 99.5%), $HAuCl_4 \cdot 3H_2O$ (> 99.9%) and (3-Mercaptopropyl)trimethoxylane (MPTES) were purchased from Sigma-Aldrich. Ethanol (Absolute), Acetone (> 99.0%), Isopropanol (> 99.5%), hydrogen peroxide (H_2O_2, 30%) and toluene (spectroscopy grade) were supplied by Merck. Ammonia (NH_3, , 28%) was purchased from Ajex Finechem. All chemicals were used without further purification. Ultrapure water (Milli-Q, R> 18.2 MΩ·cm) was used throughout.

2.2. Instrumental

Electron microscopy was carried out at the Melbourne Centre for Nanofabrication (MCN) on an FEI Helios NanoLab 600 FEG scanning electron microscope (SEM).

2.3. Synthesis of gold plates

Gold nanoparticles were synthesized via a modification of the procedure reported by Guo et al. (2006) [20]. In a typical synthesis, 50 mL of $HAuCl_4 \cdot 3H_2O$ in ethylene glycol (0.036 mmol) was degassed with nitrogen for 20 minutes. This solution was heated to 60-65°C and held at this temperature for 20 minutes. A solution of degassed aniline in ethylene glycol (720 μL, 0.1 M) was then added. The reaction mixture was left at 60-65°C for 3 hours. Following cooling, the reaction mixture was allowed to age for 3 days. Ethanol (5 mL) was added to the flask and the mixture was sonicated for 10 minutes. The dispersion was then filtered through a syringe filter (PTFE membrane with 0.2 µm pore size) and the plates collected by the filter membrane removed by washing with ethanol. The resulting plate dispersion was centrifuged for 20 min at 3000 rpm and re-dipsersed in ethanol, this was repeated twice.

2.4. Sample preparation

ITO-coated glass slides were cleaned via sonication in isopropanol for 20 minutes, then sonication in water for 20 minutes. The surface of the ITO slides were functionalized with MPTES. For this, the substrate was immersed in a solution of NH_3, H_2O_2 and water in a 1:1:5 volume ratio, and

Optics EXPRESS

this solution was heated at 70°C for 20 minutes. The slides were rinsed with water and dried thoroughly with nitrogen, followed by immersion in a solution of MPTES in toluene (1%) at 60°C for 4 minutes. The substrate was then rinsed with toluene and dried under nitrogen. The solution of nanoplates (75 μL) was spin coated onto the slide at 1000 rpm for 1 minute. Following this, the sample was soaked in ethanol for 20 minutes and dried under nitrogen.

2.5. NSOM

NSOM scans were performed on a modified MultiView 4000 (Nanonics Imaging). All scans were performed using a metal-coated optical fibre probe with a 250 nm aperture. The optical fibre was concurrently used as an AFM cantilever allowing correlation of the particle morphology with the collected light (near-field) signal. Samples were irradiated from below, through the supporting substrate with a 640 nm polarized laser (Dragon Lasers 640M20), focussed onto the surface of the sample with a 10x objective (Nikon LU Plan Fluor, 10x/0.3) at powers ranging from 0.5 to 2 μW at the back of the objective. The polarization angle was controlled by rotating a half-wave plate (Thorlabs AHWP05M-600) in the light path prior to the objective. The NSOM signal was detected using a Photomultiplier tube (PMT - PerkinElmer MP962).

2.6. Theoretical

A general treatment of surface plasmon modes in multi-layer films [21] leads to a solution for the plasmon electric field as a propagating wave at the metal surface with a wavenumber α. When this method is applied to the excitation of a plasmon from a complicated boundary, the electric field at the top surface $z \geq 0$ (where z is the top surface of the metal plate) can be written in the form [19]

$$\mathbf{E}_p(\mathbf{r}, z, t) = E_L e^{-\gamma z - i\omega t} \int \left(\frac{i\gamma \hat{r}'_s - \alpha \hat{z}}{k} \right) (\hat{e} \cdot \hat{n}') \, H_0^{(1)}(\alpha r'_s) d^2 r', \tag{1}$$

where $H_0^{(1)}(\alpha r'_s)$, the Hankel function of the first kind, represents a two-dimensional "spherical" wave at position $\mathbf{r}$ emitted from a point $\mathbf{r}'$ on the boundary. The vector distance to the point of observation from the boundary is $\mathbf{r}'_s = \mathbf{r} - \mathbf{r}'$ and the boundary normal in the $x - y$ plane at $\mathbf{r}'$ is $\hat{n}'$. The factor γ is defined by $\gamma^2 = \alpha^2 - \epsilon_d k^2$ where ϵ_d is the relative permittivity of the surrounding dielectric, $k = \omega/c$ is the free-space wavenumber with ω the frequency of the incident light that excites the plasmon and c the speed of light in vacuum. Since the NSOM measurement is made close to the surface, $z \approx 0$. We note that γ has been defined here to make the imaginary part explicit and therefore γ is a real number.

The amplitude of the plasmon wave E_L is related to the electric field of the incident light. For normally incident light, this electric field has a polarization in the plane of the metal surface with a vector $\hat{e}$. For incident light linearly polarized at angle ψ, then $\hat{e} = \cos\psi \hat{x} + \sin\psi \hat{y}$ and for circular polarization $\hat{e} = (\hat{x} \pm i\hat{y})/\sqrt{2}$ where the $\pm$ sign determines the helicity. The light field incident on an edge or a ridge of the metal platelet creates a surface charge $\sigma \propto (\epsilon_d - \epsilon_m)\hat{e} \cdot \hat{n}'$ proportional to the difference in the dielectric permittivities of the external medium ϵ_d and the metal ϵ_m, which leads to the factor $E_L(\hat{e} \cdot \hat{r}_n)$ in Eq. (1). It is clear, then, that the plasmon wave amplitude depends on the polarization properties of the incident light field. The integral in Eq. (1) is taken over the surface of the platelet, but since the source of plasmon waves is the boundary, the integral reduces to a line integral over the boundary.

In general Eq. (1) must be evaluated numerically for any complicated platelet. To understand the general features of this plasmon wave an approximate solution can be written in the case of a connected set of straight-line boundaries. For an infinite straight line boundary, it can be shown that Eq. (1) yields a plane wave solution [4] (although for our simulations in the following section we evaluate Eq. (1) numerically). Then the n-th straight line on the boundary can be represented approximately as a source of plasmon plane-waves with electric field $\mathbf{E}_{pn}$. Including the effects

Optics EXPRESS

of the incident light field ($\mathbf{E}_L$), the total electric field at the surface of the platelet is given by

$$\mathbf{E}_T = \mathbf{E}_L + \sum_n aE_L(\hat{e}\cdot\hat{r}_n)\left(\frac{i\gamma\hat{r}_n - \alpha\hat{z}}{k}\right)e^{i\alpha r_n - \gamma z}, \tag{2}$$

where the common factor of $\exp(-i\omega t)$ has been omitted. From this equation, the intensity measured at some distance z near the surface and normalized by the light at the surface can be written in the form

$$\begin{aligned}\frac{I_T}{|E_L|^2} &= 1 - 2\frac{a}{k}\sum_n(\hat{e}\cdot\hat{r}_n)^2 e^{-\alpha'' r_n - \gamma z}\gamma\hat{r}_n \sin\alpha' r_n \\ &+ \left(\frac{a}{k}\right)^2(\gamma^2 + |\alpha|^2)\sum_n(\hat{e}\cdot\hat{r}_n)^2 e^{-2\alpha'' r_n - 2\gamma z} \\ &+ 2\left(\frac{a}{k}\right)^2(\gamma^2 + |\alpha|^2)\sum_{n>m}(\hat{e}\cdot\hat{r}_n)(\hat{e}\cdot\hat{r}_m)(\hat{r}_n\cdot\hat{r}_m)e^{-\alpha''(r_n+r_m)-2\gamma z}\cos\alpha'(r_n - r_m).\end{aligned} \tag{3}$$

where $\hat{e}\cdot\hat{z} = 0$ and $\hat{e}$ is real, which assumes linear polarization. The plasmon wavenumber component γ is assumed to be real and $\alpha = \alpha' + i\alpha''$ is split into real and imaginary components but the imaginary part has cancelled out.

This equation demonstrates two sources of interference. Firstly there is a standing wave pattern created by the interference of a plasmon with the incident light field that has penetrated the metal platelet, as given by the $\sin\alpha' r_n$ dependence of the intensity. Secondly there is the interference caused by the overlap of plasmons excited from different boundaries, which is given by the $\cos\alpha'(r_n - r_m)$ term. The interference sits on top of a constant background. Note that the NSOM may only accept light that is polarized parallel to the fibre interface, or perpendicular to the fibre surface normal. In this case we should only keep the $\hat{r}_n$ component in Eq. (2) when we take the intensity. Then the measured intensity in Eq. (3) will be missing the $|\alpha|^2$ term. Nevertheless, the interference pattern will look similar.

To simulate the NSOM measurements, the gold plate boundary is represented by a series of straight lines where each point on each line is a source of outwardly propagating circular waves on the metal surface, as in Eq. (1). These are Huygen's wavelets. The total field at any point on the surface is then given by summing all wave sources around the boundary, which is equivalent to evaluating the integral. Note that thin metal films support two plasmon modes, a long range mode and a short range mode. It is straightforward to include both modes in the simulation, although one has to guess at the relative excitation strengths of each mode by the incident light field. For each point on the surface of the metal platelet, the contribution of each plasmon source to the total electric field is evaluated including the uniform incident light field. The NSOM measurement is then given by the intensity of the electric field at each point.

Optics EXPRESS

3. Results and discussion

Chemically synthesized plates [20] are crystalline with flat top and bottom facets (SEM shown in Fig. 1(a)). They are up to 10 µm across, with a range of shapes, and typically around 80 nm high. The exact morphology and height of each plate is measured via AFM during the optical measurements. We note however that the edge facets for these structures are not flat but are generally tilted at different angles with respect to the top and bottom surfaces.

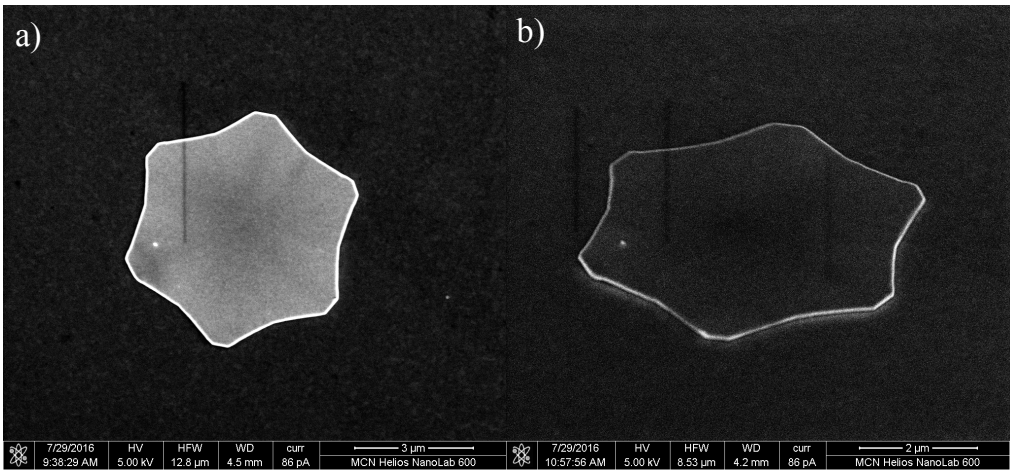

Fig. 1. Representative SEM micrographs of a plate a) at zero degrees and b) at 52 degrees tilt with respect to the incoming electron beam.

Figures 2(c) and 2(d) show the experimentally measured distribution of energy on a triangular plate when plasmons are excited at all edges for horizonal and vertical polarization of the excitation light. The panels Figs. 2(e) and 2(f) are the same NSOM scan as Figs. 2(c) and 2(d) respectively, but presented with different contrast to highlight the near-field intensity within the plate. Figures 2(a) and 2(b) show the atomic force microscopy (AFM) images collected simultaneously with the NSOM signal of the triangle.

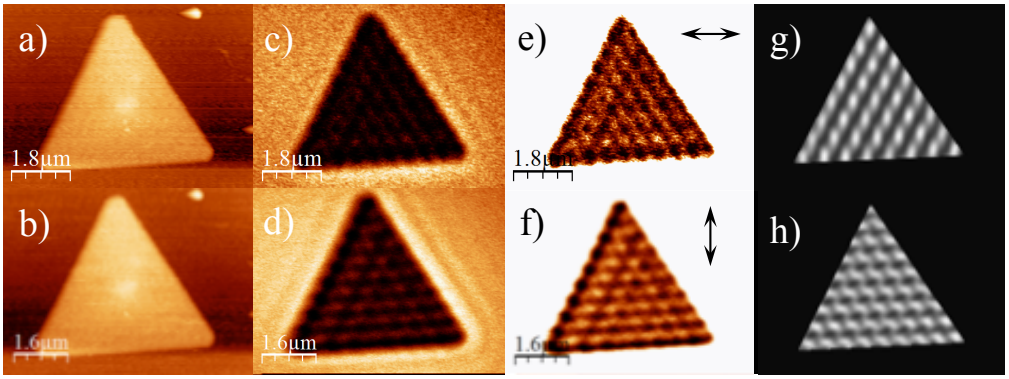

Fig. 2. (a & b) AFM scans; (c & d) NSOM scans; (e & f) intensity saturated NSOM scans; (g & h) simulated NSOM patterns, for a triangular gold plate irradiated with polarized laser light (640nm). Polarization indicated by arrows in (e) & (f).

Optics EXPRESS

Areas of enhanced near-field intensity are present across the surface of the plate. It can be seen that although there is a minor shift in the appearance of the interference pattern as a result of a 90 degree change in the polarization of the excitation light, the periodicity remains the same. More specifically, the NSOM signal for this structure has nine crests across the surface of the plate (along the axis of polarization) and the nodes are similarly localized irrespective of the polarization. However, the node pattern is not symmetrical with respect to the three edges of the triangle.

Surface plasmon polaritons at the edge of the plates are excited upon laser irradiation and these propagate radially from the excitation position. The propagation distance is a function of the material dielectric and crystallinity and the plasmon propagation length of crystalline gold nanowires has been reported to be of the order of 2 - 3 μm [22]. Therefore, for these gold plates, the waves propagate across the surface to the opposing boundary prior to the decay of the SPP, where they generally reradiate light to the far-field and possibly reflect as discussed below. The number of wave peaks observed across a structure is a function of the particle width and the wavelength of the plasmon (in the dielectric environment).

Under the experimental conditions used here, the laser spot irradiates the full plate and incoupling occurs at all points along the edge, effectively launching a plane wave from every boundary. The node pattern is thus reminiscent of the shape of the plate (Fig. 2), and independent of the probe scan direction. The nodes are aligned perpendicularly to the electric field component of the incoming light, this means the long axis of a given node is aligned with the wavefront generated by excitation dictated by the polarization of the incoming light. As a result, this makes it appear as though the waves are being projected primarily from one edge. This effect is caused by the dependence of the excitation of the plasmon waves on the vector direction of the incident field and the normal to the boundary, as determined by the term $\hat{e} \cdot \hat{n}$ in Eq. (1), making the waves in this direction appear more resolved. This demonstrates the importance of control over excitation conditions. Theoretical simulations, presented for this plate in Figs. 2(g) and 2(h), largely match the experimental near-field and this remains true when that polarization angle of the irradiating light is changed.

However, there are also some features in the experimental SNOM scans that are absent in the simulated data. Specifically these are brighter regions and slight overall pattern shift and/or discontinuity. These effects are clearest in Fig. 2(f) along the top-left edge of the triangle. There are two likely contributors to the observed pattern skewing. First is that these plates are not prisms in the sense that the edge facets are not perpendicular to the top and bottom facets. Further, the different edge facets for a single plate are not always tilted to the same angle. This would cause a disparity in the in-coupling efficiency and would be observable as skewing to the pattern intensity along the axis between higher and lower efficiency in-coupling facets. The second factor is that the size of a plate is not necessarily a multiple of the supported plasmon wavelength. This would likely appear as an irregularity in wave spacing and intensity, or a blurring of features in the NSOM scan. These contributions are expected to also be most obvious for simpler structures with few edges such as the triangle shown in Fig. 2. SPPs excited at one edge of a plate have been detected as far field radiation on the opposing side of the plate [6, 7]. SPPs may also be reflected from boundaries. The simulations do not include plasmon reflections, and the agreement between the simulated interference patterns and the experimental data implies that the proportion of energy redirected by reflection is minimal. This supports the assignment of the optical signal being the result of SPP interference rather than LSP standing waves. This also precludes assignment of this phenomenon as an LSP higher order resonance, unlike that observed for smaller particles [10].

As the observed near-field nodal (and anti-nodal) patterns are dictated by the boundary conditions imposed by the material extent, this pattern would be expected to change with the shape of the particle. And indeed this is observed. Figures 3(a)-3(d) show the AFM, Figs. 3(e)-3(h) show the experimentally measured NSOM, and Figs. 3(m)-3(p) simulated NSOM signal for a

Optics EXPRESS

series of plates with different shapes. To demonstrate the agreement between the experimental and simulated NSOM across a wide variety of shapes, Figs. 3(i)-3(l) show transparent (40%) overlays of the simulated NSOM over the experimental NSOM.

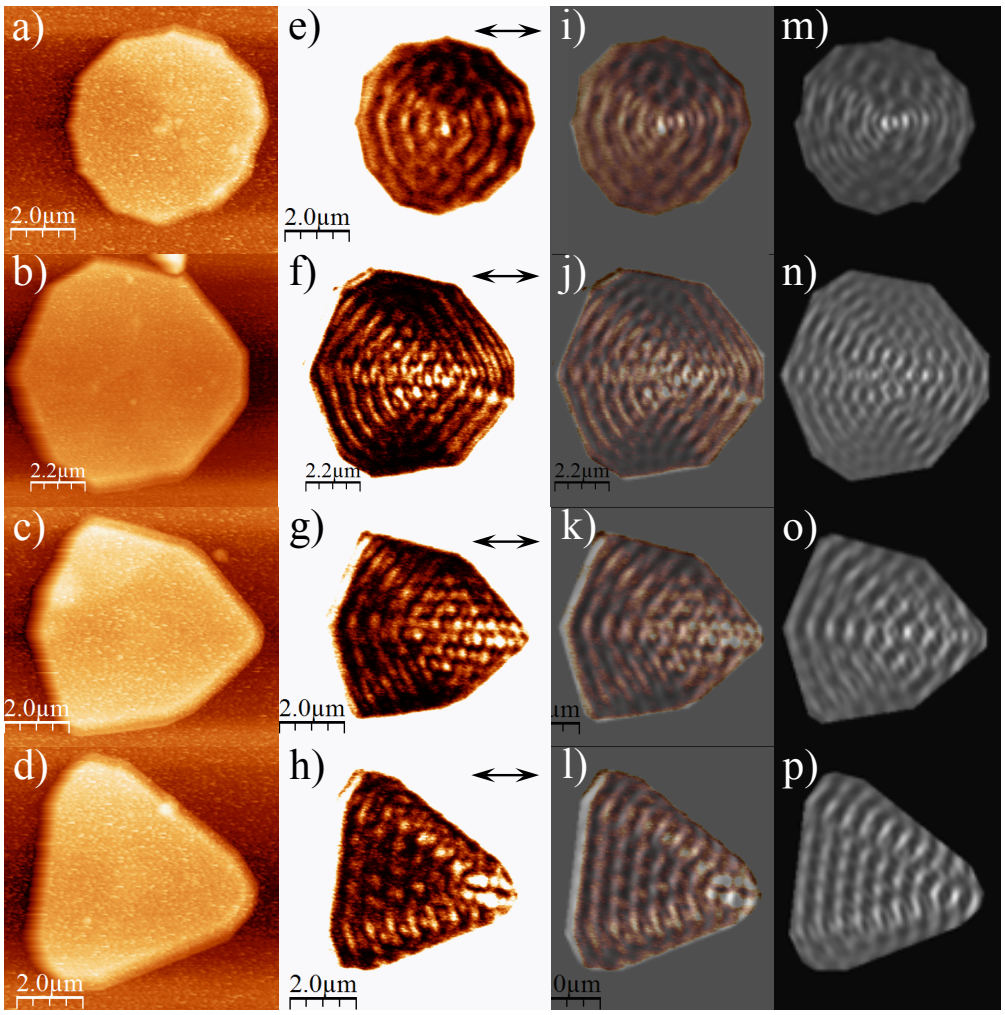

Fig. 3. (a-d) AFM scans; (e-h) intensity saturated NSOM scans; (i-l) intensity saturated NSOM scans with partially transparent overlays containing simulated NSOM patterns; (m-p) simulated NSOM patterns, for gold plates irradiated with polarized laser light (640nm). Polarization indicated by arrows in (i-l).

Figure 3 also demonstrates the effects of the shape transition from a circular plate to a triangular plate. It should be noted that the number of nodes across a plate will vary with the plate size. However, it can be observed that over the transition, more of the energy is gradually shifted from the centre of the plate toward the edges.

For all of these plates, simulations accurately reproduce the wave spacing and general features such as bright and dark areas. This demonstrates that interference patterns can be faithfully represented by this model for a wide variety of boundary conditions.

As noted above, another factor that affects the energy distribution is the polarization of the

Optics EXPRESS

exciting light. This effect is demonstrated in Fig. 4, which shows how the near field interference pattern evolves with respect to changes in the irradiation conditions, or more specifically, modification of the polarization of the irradiating light on the energy distribution for a shield-shaped plate. When the polarization axis is in line with two corners, there is more concentration of the energy in that axis. In contrast when the polarization axis crosses a corner and the opposing edge, the energy is more distributed over the surface. However, the energy distribution always rotates symmetrically with respect to the polarization angle, as is evident from the similarity between the NSOM scans for symmetrical irradiation states.

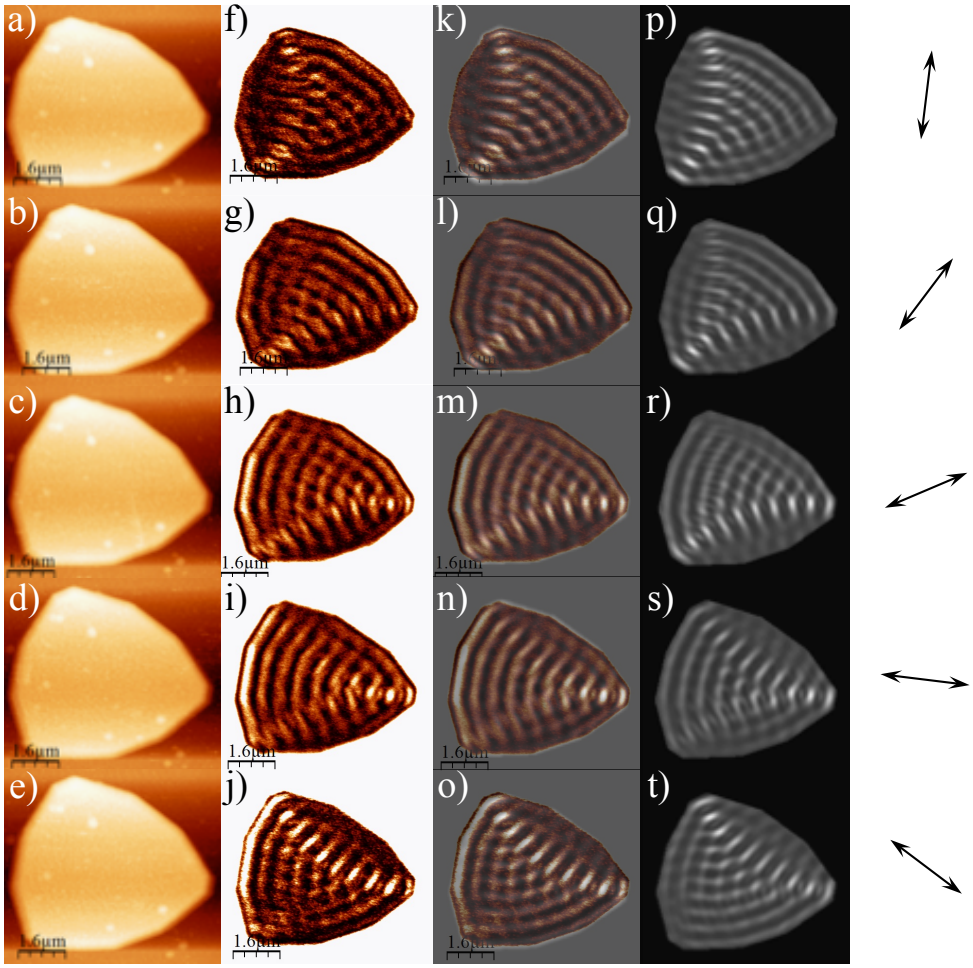

Fig. 4. (a-e) AFM scans; (f-j) intensity saturated NSOM scans; (k-o) intensity saturated NSOM scans with partially transparent overlays containing simulated NSOM patterns; (p-t) simulated NSOM patterns, for a single shield-shaped gold plate irradiated with polarized laser light (640nm). Polarization indicated by the arrows on the right.

From the AFM scans, it can be seen that this plate is composed of a series of straight line boundaries and this dictates the basic distribution for the node pattern. In the case of this shield-shaped plate, there is a more pronounced response to changes in the polarization of the irradiating light than for the triangular plate shown in Fig. 2. This is because excitation efficiency

Optics EXPRESS

is dictated by the angle between the light's polarization and the boundaries of the plate. Because the shield is a more rounded shape, this allows for a more variable distribution in available excitation efficiencies for different polarization angles. This results in a greater clarity of the near field pattern when modifying the polarization.

As such, this structure demonstrates the ability to direct plasmons through complementary control over the boundary conditions and polarization, allowing energy to be concentrated, diffused, or shifted around a structure. Furthermore, the close matches between the experimental and simulated near field maps show that the optical properties of meso-scale plasmonic devices can be predicted in a robust fashion.

4. Conclusion

In this paper, we used NSOM to characterize the near field optical response of gold microplates with thicknesses under 100 nm. A comparison between these data and simulations show high fidelity matches across a number of differently shaped plates and varying excitation polarization angles. We show experimentally how polarization control may be used to direct energy distribution and how the near field response may be predicted. This combination of experimental and simulated near field mapping affords an understanding of the structure-property relationship of this kind of mesoscale system on surface plasmons. By providing a means to accurately predict the effects of modification of boundary conditions and excitation polarization on a structure's optical properties, these results allow for multiple avenues of design for optical components.

Funding

Australian Research Council (ARC) Grants CE170100026 and DP140103011.

Acknowledgments

This work was supported by the Australian Research Council (ARC) Grants CE170100026 and DP140103011. The authors acknowledge use of facilities within the Monash Centre for Electron Microscopy.